

Coupled inductors-based interleaved boost converters for Fuel Cell Electric Vehicles

Meryem Benzine, Issam Salhi, Arnaud Gaillard, Fei Gao

UTBM, CNRS, Institut FEMTO-ST, F-90010 Belfort cedex, France

E-mails: {meryem.benzine, issam.salhi, arnaud.gaillard, fei.gao}@utbm.fr

Abstract—Fuel cell (FC) is an energy conversion device of zero-emission. It has been increasingly used in many applications, especially in Fuel Cell Electric Vehicles (FCEVs) that use the Proton Exchange Membrane Fuel Cell (PEMFC) as the main power source. Due to the low and unregulated FC stack output voltage, a DC/DC converter is required to boost and regulate the DC bus voltage to a constant value. Reliability and continuity of service remain a major challenge for FCEVs to stand out in the transportation market. In this context, the DC/DC converter should ensure operational safety while increasing power density. Since using coupled inductors can improve the efficiency and reduce size and volume of converters, a comparison study is considered in this paper between different four-phase interleaved boost converter (4IBC) topologies, in both healthy and faulty operation modes. Simulation results show that, compared to the loosely coupled inductors and uncoupled inductors, the cascade cyclic coupled structure is very advantageous in terms of current ripple reduction, which make it well qualified for FCEVs.

Index Terms—DC/DC interleaved Boost Converter, coupled inductors, cascade cyclic, loosely coupled, switch-fault, Fuel Cell Electric Vehicle.

I. INTRODUCTION

Fuel cell electric vehicles (FCEVs) are among the devices that have emerged in recent years [1]. One of the attractive power supply source is the proton exchange membrane fuel cell (PEMFC) due to its zero emissions, high energy efficiency, and relatively low operating temperature [2]. Since the PEMFC is a high current but low voltage source, a DC/DC boost converter is required to regulate the output voltage to a fixed DC bus voltage as shown in the example of the FCEV powertrain shown in Fig. 1. A secondary energy source, such as battery or supercapacitors, is also essential. It helps not only to manage power transients but also to store the lost energy during braking, as in Toyota Mirai [3].

The most important requirements for selecting a suitable converter for FCEVs are : high efficiency, high power density, low cost, high reliability, and low current ripple. The interleaved boost converter (IBC), presented in Fig. 2(a), is known as one of the enhanced non-isolated boost converters that is well suited to FCEVs [4]–[8]. It has been shown that the current ripples are greatly reduced when increasing the number of phases. However, as the number of phases increases, the volume of magnetic components increases as well. Using coupled inductors instead of uncoupled inductors,

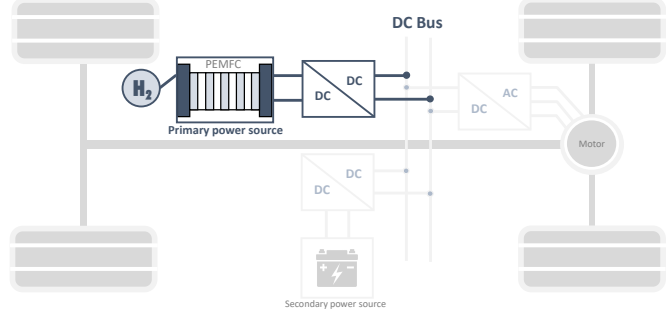


Fig. 1. Powertrain of a Fuel Cell Electric Vehicle

would help reduce the cost, size, and losses of interleaved boost converters. From the efficiency point of view, like in Toyota Mirai [3], four phases are considered to be enough to ensure good performances [4].

On the other hand, maintaining reliability and service continuity of the converter is a major challenge for the FCEVs. Based on a study [8], switches are the most fragile components of DC/DC converters. Thanks to the switches redundancy, the IBC offers the possibility to operate in degraded mode in case of a switch failure. Thus, continuity of service could be guaranteed. However, even if coupled inductors bring advantages in healthy mode, the question of reliability remains one of the major issues. Indeed, the isolation of the faulty phase can affect the other healthy phases as they are coupled.

A judicious choice of the coupling structure remains necessary in order to propose a fault-tolerant converter adapted to FCEVs applications. For this purpose, this paper presents a comparison between the coupling structures (cascade cyclic and loosely coupled inductors) and the uncoupled structure of interleaved multiphase converters, in both healthy and faulty operation. Simulations were performed, using Simpower System tool of Matlab / Simulink, in open-loop and closed-loop for the three previously mentioned topologies. The three architectures are compared in terms of current/voltage ripples. The cascade cyclic structure was shown to be the best performing architecture whether in healthy or faulty mode.

The rest of the paper is organized as follows: in Section II, a generality about type and structures of coupling is presented. The cascade cyclic structure is analysed in Section III. In Section IV, simulation results of the comparison between separate inductors and two type of coupling structures, loosely

This work has been supported by the EIPHI Graduate School (contract ANR-17- EURE-0002), the Region Bourgogne Franche-Comté and the Moroccan Ministry of Higher Education, Scientific Research and Innovation.

and cyclic cascade are presented. The Section V concludes the paper with some final remarks.

II. BOOST CONVERTERS WITH COUPLING STRUCTURE

Magnetic components are among the components that occupy more space and have an important weight in the FCEVs. Since volume and weight are critical factors for FCEVs, the use of coupled inductors is highly recommended to improve electrical performance and reduce size and weight. There are two coupling types and various coupling structures.

A. Type of coupling

The coupling of the inductors can be realized in two ways: in direct or inverse. The inverse-coupled configuration cancels the majority of the flux generated in the core because of opposite polarity of the generated flux of the two coupled windings [9]. Nevertheless, in the direct-coupled configuration, the flux generated by the two windings is summed rather than canceled in the core. Consequently, direct-coupled configurations will more easily saturate the core when operating under high-output current conditions [9]. The inverse-coupled configuration has been used in various applications to reduce magnetic volume and to improve performances, especially in the interleaved buck/boost converters [9]–[10]. It is the best choice for high power interleaved boost converters.

B. Coupling structures

There are several coupling structures for multiphase converters. Among the structures most popular in literature, is the monolithic structure where all the phases are wound on the same and unique magnetic core. It has been suggested as a good low volume structure [11]–[13]. However, it requires complex magnetic structures to be realized in practice. Its major drawback is when a fault appear in a certain phase, it will directly affects the others branches by creating inductors' current imbalance in the inductors, which considerably complicates its control.

Loosely coupled inductors is a structure which reduce to half the number of cores in an uncoupled-inductors topology. In the case of a four-phase IBC, only two cores will be needed. Each core has two windings of two phases on the outer legs [14]. It offers a lower volume. The mutual coupling exists only between two phases as shown in Fig. 2(b). The voltage equations of the four-phase inductors in Fig. 2(b) are expressed as

$$\begin{bmatrix} V_{L_1} \\ V_{L_2} \\ V_{L_3} \\ V_{L_4} \end{bmatrix} = \begin{bmatrix} L_1 & 0 & -M_{31} & 0 \\ 0 & L_2 & 0 & -M_{42} \\ -M_{13} & 0 & L_3 & 0 \\ 0 & -M_{24} & 0 & L_4 \end{bmatrix} \frac{d}{dt} \begin{bmatrix} i_{L_1} \\ i_{L_2} \\ i_{L_3} \\ i_{L_4} \end{bmatrix} \quad (1)$$

Intercell transformers (ICT) is a structure of symmetrically coupled inductors, it can be built from multiple two-winding coupled inductors [15]. The most commonly used architecture is the cascade cyclic structure, as in [15]–[18]. Mutual coupling only exists between adjacent phase legs. Two inductors are used in each phase. Each one links the current of one leg to the current of the next, except for the last which is

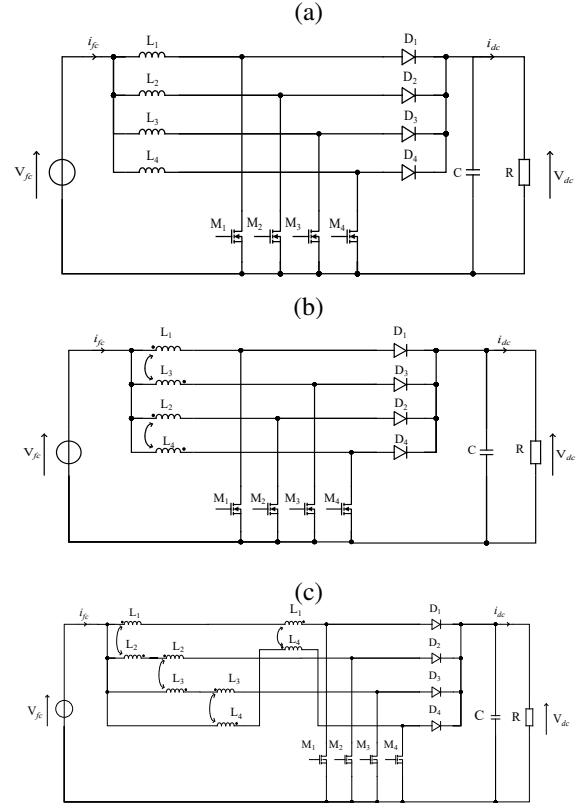


Fig. 2. 4IBC electrical circuits, (a) Uncoupled, (b) Loosely coupled, (c) Cascade cyclic

linked to the first, as illustrated in Fig. 2(c). It is less bulky than the structures that require a large number of transformers such as the combinatorial cascade structure as in [16]. The cascade cyclic structure is easy to design, it can be realized by assembling standard cores. The use of separate transformers in case of failure is attractive because the saturation will be locally situated in the concerned phases elementary ICT [19].

The voltage equations of the four-phase inductors in Fig. 2(c) are expressed as

$$\begin{bmatrix} V_{L_1} \\ V_{L_2} \\ V_{L_3} \\ V_{L_4} \end{bmatrix} = \begin{bmatrix} 2L_1 & -M_{21} & 0 & -M_{41} \\ -M_{12} & 2L_2 & -M_{32} & 0 \\ 0 & -M_{23} & 2L_3 & -M_{43} \\ -M_{14} & 0 & -M_{34} & 2L_4 \end{bmatrix} \frac{d}{dt} \begin{bmatrix} i_{L_1} \\ i_{L_2} \\ i_{L_3} \\ i_{L_4} \end{bmatrix} \quad (2)$$

For a symmetric magnetic core ($L_1 = L_2 = L_3 = L_4 = L$), the mutual inductances are also equal ($M_1 = M_2 = M_3 = M_4 = M$). The coupling coefficient is defined as $k = \frac{M}{L}$. The Table I summarizes the comparison between the coupling structures in terms of design and control complexity [19].

III. CYCLIC CASCADE COUPLED INDUCTORS 4IBC

In the IBC with cyclic cascade coupled inductors, presented in Fig. 2(c), the four switches are controlled with the same duty cycle and shifted by $T_s/4$, where T_s is the switching period. There are eight operating modes in each switching cycle. Fig. 3 shows the switch control signals for $T_s/2 < d < 3T_s/4$ where d is the duty cycle.

TABLE I
COMPARISON OF TOPOLOGIES IN TERMS OF DESIGN AND CONTROL COMPLEXITY

	Uncoupled	Monolithic	Loosely	Cascade cyclic
Number of cores	4	1	2	4
Number of windings per phase	1	1	1	2
Difficulty to control in case of phase loss	Normal	Difficult	Medium	Medium

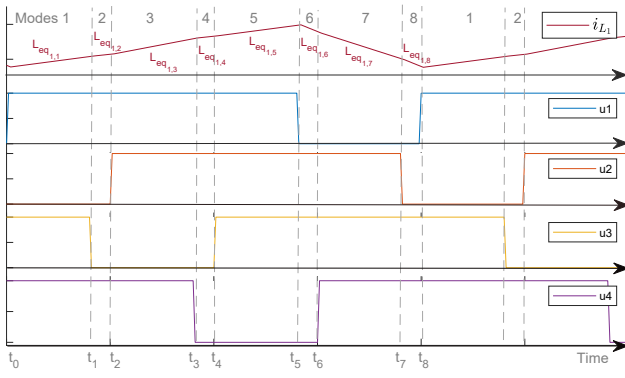


Fig. 3. Waveforms of the inductor current in phase 1 and switch control signals for ($T_s/2 < d < 3T_s/4$).

The ideal static voltage gain of the interleaved boost converter is

$$M(D) = \frac{V_{dc}}{V_{fc}} = \frac{1}{1-d} \quad (3)$$

From (2), the derivative of the inductor currents in time can be written as follows

$$\left\{ \begin{array}{l} \frac{di_{L_1}}{dt} = \frac{(2L^2 - M^2)V_{L_1} + M^2V_{L_3} + LM(V_{L_2} + V_{L_4})}{4L(L^2 - M^2)} \\ \frac{di_{L_2}}{dt} = \frac{(2L^2 - M^2)V_{L_2} + M^2V_{L_4} + LM(V_{L_1} + V_{L_3})}{4L(L^2 - M^2)} \\ \frac{di_{L_3}}{dt} = \frac{(2L^2 - M^2)V_{L_3} + M^2V_{L_1} + LM(V_{L_2} + V_{L_4})}{4L(L^2 - M^2)} \\ \frac{di_{L_4}}{dt} = \frac{(2L^2 - M^2)V_{L_4} + M^2V_{L_2} + LM(V_{L_1} + V_{L_3})}{4L(L^2 - M^2)} \end{array} \right. \quad (4)$$

During mode 1 (t_0-t_1), switches M_1 , M_3 and M_4 are ON and M_2 is OFF : $V_{L_1} = V_{L_3} = V_{L_4} = V_{fc} > 0$ and $V_{L_2} = V_{fc} - V_{dc} = \frac{-d}{1-d}V_{fc} < 0$,

From (4), $\frac{di_{L_1}}{dt}$ can be expressed as

$$\frac{di_{L_1}}{dt} = \frac{2L^2 + LM - \frac{LM}{1-d}d}{4L(L^2 - M^2)}V_{L_1} \quad (5)$$

Hence, V_{L_1} is defined by

$$V_{L_1} = L_{eq,1,1} \frac{di_{L_1}}{dt} \quad (6)$$

with

$$L_{eq,1,1} = \frac{4L(L^2 - M^2)}{2L^2 + LM - \frac{LM}{1-d}d} \quad (7)$$

Since $k = \frac{M}{L}$, $L_{eq,1,1}$ can be written as

$$L_{eq,1,1} = \frac{4(1 - k^2)}{2 - \frac{kd}{1-d} + k}L \quad (8)$$

$L_{eq,1,1}$ is the equivalent inductance of i_{L_1} for the mode 1 for $T_s/2 < d < 3T_s/4$. For each mode, there are 8 equivalent inductances.

Following the same steps, the formula of the equivalent inductance for phase 1 in other modes can be obtained,

Mode 2

$$L_{eq,1,2} = \frac{4(1 - k^2)}{2 - k^2 + k - \frac{(k + k^2)d}{1-d}}L \quad (9)$$

Mode 3

$$L_{eq,1,3} = \frac{4(1 - k^2)}{2(1 + k) - \frac{k^2}{1-d}}L \quad (10)$$

Mode 4

$$L_{eq,1,4} = \frac{4(1 - k^2)}{2 - k^2 + k - \frac{(k + k^2)d}{1-d}}L \quad (11)$$

Mode 5

$$L_{eq,1,5} = \frac{4(1 - k^2)}{2 + k - \frac{kd}{1-d}}L \quad (12)$$

Mode 6

$$L_{eq,1,6} = \frac{4(1 - k^2)(1 - d)}{(-2d + k)(1 + k)}L \quad (13)$$

Mode 7

$$L_{eq,1,7} = \frac{4(1 - k^2)}{\frac{k^2 - 2d}{1-d} + 2k}L \quad (14)$$

Mode 8

$$L_{eq,1,8} = L_{eq,1,6} \quad (15)$$

In Fig. 3, the waveform of i_{L_1} for each mode is illustrated. The equivalent inductances of phases 2, 3 and 4, for each mode, can be obtained by following the same method.

IV. COMPARISON BETWEEN THE BEHAVIOR OF DIFFERENT COUPLED INDUCTORS 4IBC

In order to study the behavior of the loosely, cascade cyclic coupled inductors and separate inductors of the 4IBC in case of switch fault, a comparison of the three topologies in open-loop and with closed-loop controller is established in Matlab/Simulink. During the simulations, the converters operate in healthy mode and then, a fault in phase 1 occurs at $t = 0.2s$. The coupling coefficient is chosen as in [20] to facilitate the core fabrication. The saturation of the inductances is not taken into account in the simulations. The rated parameters of the converter are given in Table II.

A. Open loop simulation

An open-loop simulation of four-phase interleaved boost converters with loosely, cascade cyclic, and separate inductors in case of loss of phase 1 at $t=0.2s$, is performed. Fig. 4 presents the inductor currents waveforms of the previously mentioned converters in open-loop. It has been shown that in case of a phase failure, the input current is distributed to the other healthy phases. This creates an imbalance in the phase currents, which can lead to saturation of the magnetic cores. The cyclic cascade 4IBC is the architecture that presents less current ripples before and after the appearance of the fault.

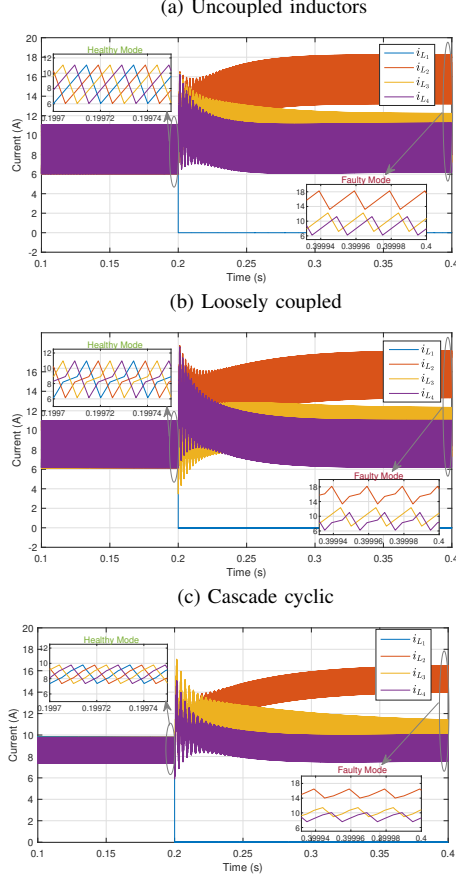


Fig. 4. Inductor currents waveforms of 4IBC with inverse coupled inductors in case of fault of phase 1 (Open-loop) at $t = 0.2s$.

TABLE II
IBC SPECIFICATIONS PARAMETERS

Parameters	Value	Unit
Output voltage (V_{dc})	48	V
Input Voltage (V_{fc})	14.4	V
Output power (P)	500	W
Switching frequency (f_s)	50	kHz
Inductor (L, r_L)	(40, 0.2)	(μ H, m Ω)
Capacity (C)	1000	μ F
Coupling coefficient (k)	-0.3	
Tolerated output voltage ripple (ΔV_{dc})	$\leq 1\%$	
Tolerated input current ripple (ΔI_{fc})	$\leq 10\%$	

B. Closed-loop control

A dual-loop PI controller is applied to each converter. The outer bus DC voltage loop generates the reference current i_L^* for all the inner current loops as shown in Fig. 5. Then, the internal loops generate the duty cycles. The PWM block produces the switching signal for the switches.

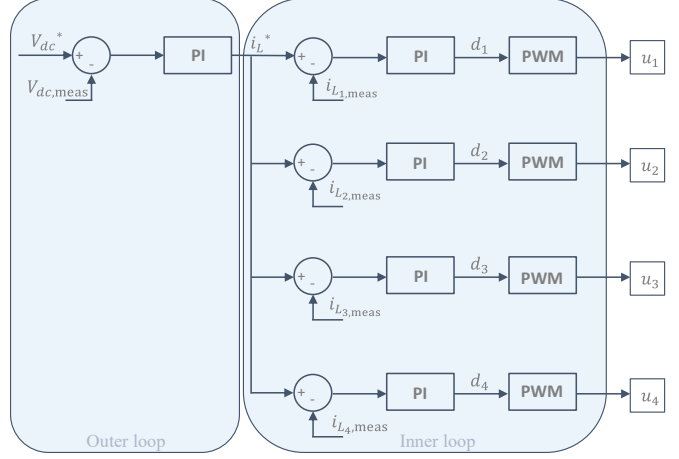


Fig. 5. Diagram of the dual-loop PI controller

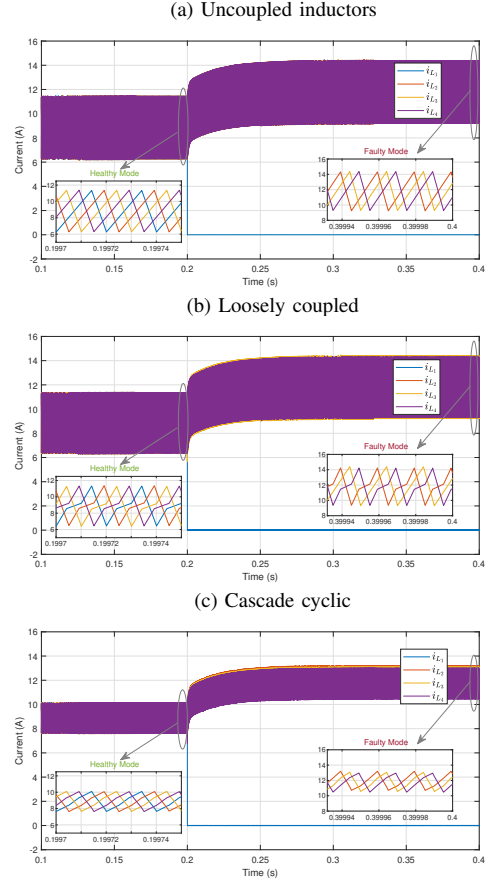


Fig. 6. Simulation results of inductors currents waveforms of converters with closed-loop control in case of switch fault at $t = 0.2s$ without phase shifting reconfiguration.

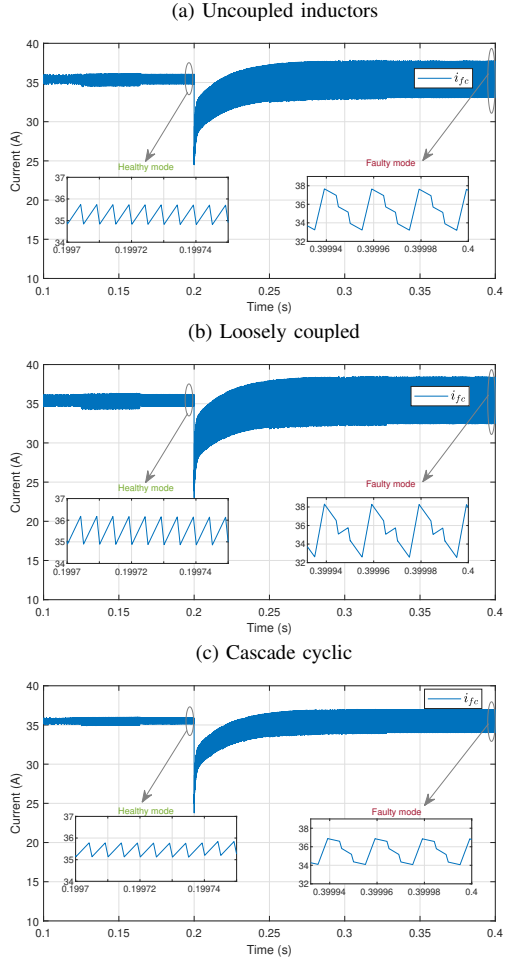


Fig. 7. Input current waveforms in closed-loop control in case of switch fault at $t = 0.2s$ without phase shifting reconfiguration.

The waveforms of inductor currents, input current and output voltage, without phase shifting reconfiguration, are shown respectively in Fig. 6, Fig. 7 and Fig. 8. It can be observed, from the aforementioned figures, that after the isolation of the failed branch, the PI controller ensures the continuity of service in degraded mode. The loss of one phase is compensated by the other three remaining healthy phases. Thus, the current delivered by the input source is then equally distributed among the healthy phases. This creates a significant increase in current ripples which increases as well the ripples in the output voltage. For this reason, a reconfiguration of phase shifting is required to reduce the input current ripple. Since the converter works with three healthy phases, the control signals of the three healthy switches should be reshifted by $T_s/3$ as shown in Table III.

Fig. 9, Fig. 10 and Fig. 11 show respectively inductor currents, input current and output voltage when the reconfiguration of the phase shifting is applied. Table IV summarizes the comparison between the different topologies in terms of current ripples, in healthy mode and faulty mode with and without the phase shifting reconfiguration. ΔI_{fc} and

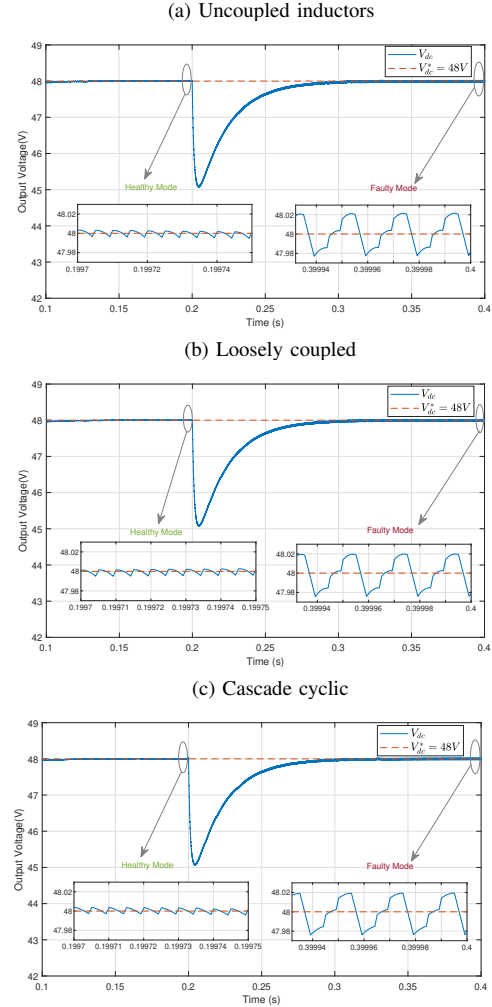


Fig. 8. Output voltage waveforms in closed-loop control in case of switch fault at $t = 0.2s$ without phase shifting reconfiguration.

ΔI_L represent, respectively, the input current ripple rate and the inductor current ripple rate. It can be noticed that the input current ripples is reduced and inductor currents become balanced. From Fig. 8 and Fig. 11, it is observed that the output voltage curve is almost the same for all topologies. Therefore, the choice of the coupling structure has no impact on the output voltage. It can be concluded that the cascade cyclic topology offers less ripples of all currents (input and inductors), in faulty and healthy modes.

V. CONCLUSION

This study presents a comparison between separate inductors 4IBC and two different topologies of coupled 4IBC: loosely and cascade cyclic. The four-phase interleaved boost with inversely cascade cyclic coupled inductors is very attractive, since it improves efficiency, and reduces input current ripples which will help to improve the lifetime of the FC. All these advantages make this architecture a better candidate for FCEVs. Fault detection of the cascade cyclic structure will be considered in future works.

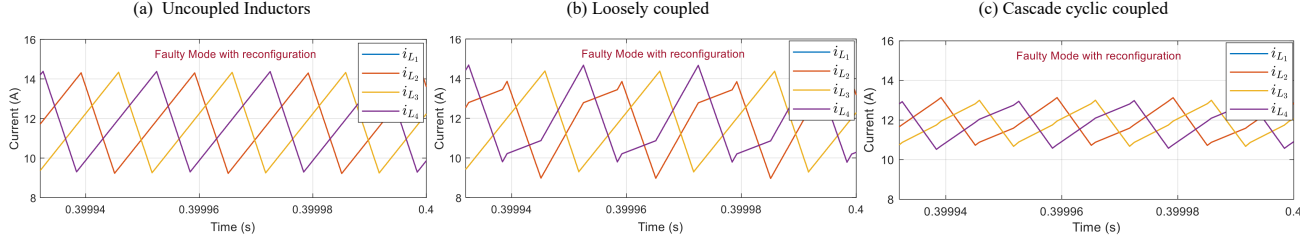


Fig. 9. Inductor currents waveforms in closed-loop control in case of switch fault at $t = 0.2s$ with phase shifting reconfiguration.

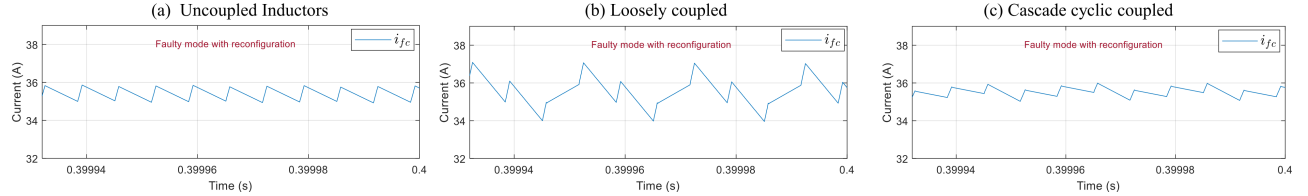


Fig. 10. Input current waveforms in closed-loop control in case of switch fault at $t = 0.2s$ with phase shifting reconfiguration.

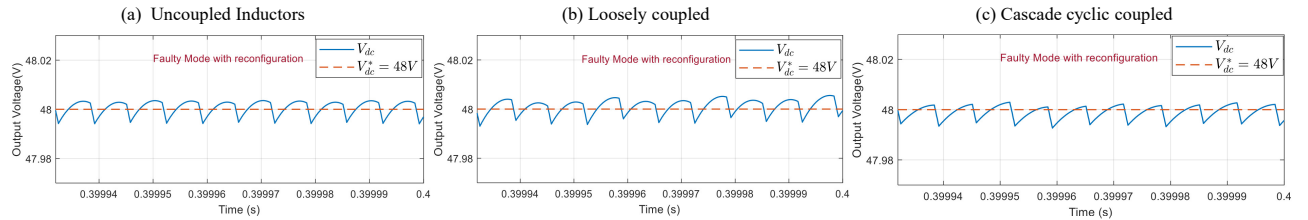


Fig. 11. Output voltage waveforms in closed-loop control in case of switch fault at $t = 0.2s$ with phase shifting reconfiguration.

TABLE III
PHASE SHIFTING IN HEALTHY AND FAULTY MODES

	Phase shifting			
	Phase 1	Phase 2	Phase 3	Phase 4
Healthy Mode	0	$\frac{T_s}{4}$	$\frac{T_s}{2}$	$\frac{3T_s}{4}$
Phase 1 fault	/	$\frac{T_s}{4}$	$\frac{7T_s}{12}$	$\frac{11T_s}{12}$
Phase 2 fault	T_s	/	$\frac{4T_s}{3}$	$\frac{5T_s}{3}$
Phase 3 fault	T_s	$\frac{4T_s}{3}$	/	$\frac{5T_s}{3}$
Phase 4 fault	T_s	$\frac{4T_s}{3}$	$\frac{5T_s}{3}$	/

TABLE IV
COMPARISON OF TOPOLOGIES WITH CLOSED-LOOP CONTROL

	Healthy Mode			Faulty Mode			
				Without reconfiguration		With reconfiguration	
	Uncoupled	Loosely	Cascade cyclic	Uncoupled	Loosely	Cascade cyclic	
$\Delta i_{fc}(\%)$	2.5%	3.55%	1.8%	12.47%	14.89%	7.8%	2.3% 8.6% 2.3%
$\Delta i_L(A)$	5.05	4.84	2.429	5.05	4.84	2.48	5.036 4.85 2.39

REFERENCES

- [1] H. N. Tran, T.-T. LE, H. Jeong, S. Kim, and S. Choi, "A 300 khz, 63 kw/l zvt dc–dc converter for 800-v fuel cell electric vehicles," *IEEE Transactions on Power Electronics*, vol. 37, no. 3, pp. 2993–3006, 2022.
- [2] B. Geng, J. K. Mills, and D. Sun, "Two-stage energy management control of fuel cell plug-in hybrid electric vehicles considering fuel cell longevity," *IEEE Transactions on Vehicular Technology*, vol. 61, no. 2, pp. 498–508, 2012.
- [3] "Toyota mirai 2021," <https://www.toyota-europe.com/world-of-toyota/feel/environment/better-air/fuel-cell-vehicle>.
- [4] M. Kabalo, D. Paire, B. Blunier, D. Bouquain, M. G. Simoes, and A. Miraoui, "Experimental validation of high-voltage-ratio low-input-current-ripple converters for hybrid fuel cell supercapacitor systems," *IEEE Transactions on Vehicular Technology*, vol. 61, no. 8, pp. 3430–3440, 2012.
- [5] D. Wang, Z. Wang, Z. Peng, Y. Zhang, and X.-F. Cheng, "A four-phase interleaved buck-boost converter with changed load connection for the fuel cell activation," *IEEE Access*, vol. 9, pp. 102 104–102 113, 2021.
- [6] J. Guo, R. Rodriguez, J. Gareau, D. Schumacher, M. Alizadeh, P. Azer, J. Bauman, B. Bilgin, and A. Emadi, "A comprehensive analysis for high-power density, high-efficiency 60 kw interleaved boost converter design for electrified powertrains," *IEEE Transactions on Vehicular Technology*, vol. 69, no. 7, pp. 7131–7145, 2020.
- [7] P. Mungporn, P. Thounthong, B. Yodwong, C. Ekkaravarodom, A. Bilsalam, S. Pierfederici, D. Guilbert, B. Nahid-Mobarakeh, N. Bizon, Z. Shah, S. Khomfoi, P. Kumam, and P. Burikham, "Modeling and control of multiphase interleaved fuel-cell boost converter based on hamiltonian control theory for transportation applications," *IEEE Transactions on Transportation Electrification*, vol. 6, no. 2, pp. 519–529, 2020.
- [8] S. Zhuo, A. Gaillard, L. Xu, C. Liu, D. Paire, and F. Gao, "An observer-based switch open-circuit fault diagnosis of dc–dc converter for fuel cell application," *IEEE Transactions on Industry Applications*, vol. 56, no. 3, pp. 3159–3167, 2020.
- [9] H. Kosai, S. McNeal, B. Jordan, J. Scofield, B. Ray, and Z. Turgut, "Coupled inductor characterization for a high performance interleaved boost converter," *IEEE Transactions on Magnetics*, vol. 45, no. 10, pp. 4812–4815, 2009.
- [10] V. Samavatian and A. Radan, "A high efficiency input/output magnetically coupled interleaved buck-boost converter with low internal oscillation for fuel-cell applications: Ccm steady-state analysis," *IEEE Transactions on Industrial Electronics*, vol. 62, no. 9, pp. 5560–5568, 2015.
- [11] J. Imaoka, K. Okamoto, M. Shoyama, M. Noah, S. Kimura, and M. Yamamoto, "A high-reliable magnetic design method for three-phase coupled inductor used in interleaved multi-phase boost converters," in *2017 IEEE Energy Conversion Congress and Exposition (ECCE)*, 2017, pp. 873–880.
- [12] H. Kowatari, T. Kitamura, and N. Hoshi, "Design and evaluation of a magnetically-loosely-coupled inductor for a four-phase interleaved boost chopper," in *2018 International Power Electronics Conference (IPEC-Niigata 2018 -ECCE Asia)*, 2018, pp. 2660–2667.
- [13] L. Yu, W. Mu, C. Yang, L. Zhu, Z. Qi, L. Wang, Y. Yao, Y. Su, and C. Zhang, "Symmetric four-phase inverse coupled inductors for gan-based interleaving four-phase point-of-load converters," in *2021 IEEE Energy Conversion Congress and Exposition (ECCE)*, 2021, pp. 5453–5458.
- [14] S. Kimura, Y. Itoh, W. Martinez, M. Yamamoto, and J. Imaoka, "Downsizing effects of integrated magnetic components in high power density dc–dc converters for ev and hev applications," *IEEE Transactions on Industry Applications*, vol. 52, no. 4, pp. 3294–3305, 2016.
- [15] E. Laboure, A. Cuniere, T. A. Meynard, F. Forest, and E. Sarraute, "A theoretical approach to intercell transformers, application to interleaved converters," *IEEE Transactions on Power Electronics*, vol. 23, no. 1, pp. 464–474, 2008.
- [16] G. J. Capella, J. Pou, S. Ceballos, J. Zaragoza, and V. G. Agelidis, "Current-balancing technique for interleaved voltage source inverters with magnetically coupled legs connected in parallel," *IEEE Transactions on Industrial Electronics*, vol. 62, no. 3, pp. 1335–1344, 2015.
- [17] Q. Deng, J. Liu, D. Czarkowski, W. Hu, and H. Zhou, "An inductive power transfer system supplied by a multiphase parallel inverter," *IEEE Transactions on Industrial Electronics*, vol. 64, no. 9, pp. 7039–7048, 2017.
- [18] M. Bojarski, E. Asa, K. Colak, and D. Czarkowski, "Analysis and control of multiphase inductively coupled resonant converter for wireless electric vehicle charger applications," *IEEE Transactions on Transportation Electrification*, vol. 3, no. 2, pp. 312–320, 2017.
- [19] S. Sanchez, F. Richardeau, and D. Risaletto, "Design and fault-operation analysis of a modular cyclic cascade inter-cell transformer (ICT) for parallel multicell converters," *Mathematics and Computers in Simulation*, vol. 131, pp. 190–199, 2017, 11th International Conference on Modeling and Simulation of Electric Machines, Converters and Systems.
- [20] F. Yang, X. Ruan, Y. Yang, and Z. Ye, "Interleaved critical current mode boost pfc converter with coupled inductor," *IEEE Transactions on Power Electronics*, vol. 26, no. 9, pp. 2404–2413, 2011.